

Adhesion in flexible organic and hybrid organic/inorganic light emitting device and solar cells

D. Yu, O. K. Oyewole, D. Kwabi, T. Tong, V. C. Anye, J. Asare, E. Rwenyagila, A. Fashina, O. Akogwu, J. Du, and W. O. Soboyejo

Citation: *Journal of Applied Physics* **116**, 074506 (2014); doi: 10.1063/1.4892393

View online: <http://dx.doi.org/10.1063/1.4892393>

View Table of Contents: <http://scitation.aip.org/content/aip/journal/jap/116/7?ver=pdfcov>

Published by the [AIP Publishing](#)

Articles you may be interested in

[Adhesion and degradation of organic and hybrid organic-inorganic light-emitting devices](#)

J. Appl. Phys. **115**, 084504 (2014); 10.1063/1.4867051

[Organic-inorganic hybrid thin film solar cells using conducting polymer and gold nanoparticles](#)

Appl. Phys. Lett. **102**, 183902 (2013); 10.1063/1.4804377

[p-type doping effect on the performance of organic-inorganic hybrid solar cells](#)

Appl. Phys. Lett. **99**, 233305 (2011); 10.1063/1.3669393

[High efficiency and stability in air of the encapsulation-free hybrid organic-inorganic light-emitting diode](#)

Appl. Phys. Lett. **92**, 213304 (2008); 10.1063/1.2936300

[Effects of molecular interface modification in hybrid organic-inorganic photovoltaic cells](#)

J. Appl. Phys. **101**, 114503 (2007); 10.1063/1.2737977



AIP | Journal of
Applied Physics

Journal of Applied Physics is pleased to
announce **André Anders** as its new Editor-in-Chief

Adhesion in flexible organic and hybrid organic/inorganic light emitting device and solar cells

D. Yu,^{1,2} O. K. Oyewole,^{3,4} D. Kwabi,^{1,2} T. Tong,^{1,5} V. C. Anye,⁶ J. Asare,³ E. Rwenyagila,⁶ A. Fashina,³ O. Akogwu,^{1,2} J. Du,^{1,2} and W. O. Soboyejo^{1,2,6}

¹*Princeton Institute of Science and Technology of Materials, Princeton University, 70 Prospect Street, Princeton, New Jersey 08544, USA*

²*Department of Mechanical and Aerospace Engineering, Princeton University, Olden Street, Princeton, New Jersey 08544, USA*

³*Department of Theoretical and Applied Physics, African University of Science and Technology, Km 10, Airport Road, Galadimawa, Abuja, Federal Capital Territory, Nigeria*

⁴*Department of Materials Science and Engineering, Kwara State University, Malete, Kwara State, Nigeria*

⁵*Department of Electrical Engineering, Princeton University, Olden Street, Princeton, New Jersey 08544, USA*

⁶*Department of Materials Science and Engineering, African University of Science and Technology, Km 10, Airport Road, Galadimawa, Abuja, Federal Capital Territory, Nigeria*

(Received 16 May 2014; accepted 25 July 2014; published online 19 August 2014)

This paper presents the results of an experimental study of the adhesion between bi-material pairs that are relevant to organic light emitting devices, hybrid organic/inorganic light emitting devices, organic bulk heterojunction solar cells, and hybrid organic/inorganic solar cells on flexible substrates. Adhesion between the possible bi-material pairs is measured using force microscopy (AFM) techniques. These include: interfaces that are relevant to organic light emitting devices, hybrid organic/inorganic light emitting devices, bulk heterojunction solar cells, and hybrid combinations of titanium dioxide (TiO₂) and poly(3-hexylthiophene). The results of AFM measurements are incorporated into the Derjaguin-Muller-Toporov model for the determination of adhesion energies. The implications of the results are then discussed for the design of robust organic and hybrid organic/inorganic electronic devices. © 2014 AIP Publishing LLC.

[<http://dx.doi.org/10.1063/1.4892393>]

I. INTRODUCTION

In the recent years, there has been increasing interest in the development of organic light emitting devices (OLED) with lower power consumption and higher resolution than traditional displays.¹ Bulk heterojunction solar cells with active layers consisting of poly(3-hexylthiophene) (P3HT) and phenyl-C₆₁-butyric acid methyl ester (PCBM) have also been engineered to have efficiencies of ~10%.² However, one of the major challenges is the design of improved charge transport. This is because of the tendency for charge recombination to occur before the charges reach the electrodes. The challenges are further exacerbated by the limited adhesion and contact at the interfaces between the layers that are relevant to organic electronics structures.^{3–5}

There is, therefore, a need to engineer new ways of improving charge mobility and adhesion/contact within/between the layers that are relevant to organic solar cells and organic light emitting devices. There is also a potential for improving charge transport via incorporation of nanoscale titanium dioxide (TiO₂) particles into the active layers of organic solar cells and light emitting devices.⁶ In the case of organic solar cells, the results show that, in selected cases, the device performance may be improved, depending on the morphology and sizes of the nanoscale TiO₂ particles.⁶

McGehee⁷ has explored the fabrication of highly efficient hybrid solar cells with improved exciton and charge conduction in the bulk heterojunction solar cells. Kuo⁸ have

developed fabrication processes for the processing of hybrid organic/inorganic solar cells with well aligned TiO₂ nanorods in P3HT matrix layers. These were shown to have higher efficiencies than bilayer TiO₂ film/P3HT cells. Her⁹ has also processed hybrid photovoltaic cells with well-ordered nanoporous TiO₂/P3HT structures. These hybrid cells had higher efficiencies than traditional thin film TiO₂. Similarly, Yodyingyong¹⁰ has demonstrated higher efficiencies in hybrid solar cells with active layers containing P3HT/PCBM mixtures and highly oriented TiO₂ nanotubes with smaller diameters and larger surface areas. Kwong¹¹ has also studied the influence of TiO₂ volume fraction on (P3HT):TiO₂ nanocomposite solar cells. The device performance was found to be optimum for TiO₂ volume fractions of 50% and 60%.

Furthermore, due to the attractive characteristics of the stretchable electronics, considerable efforts have been made to design and fabricate stretchable electronic devices.^{12–14} Intrinsically stretchable polymer light emitting devices have been fabricated using carbon nanotube-polymer composite electrodes.¹⁵ These are metal-free and can be linearly stretched to strains of up to 45%.¹⁵ Stretchable organic solar cells have also been fabricated on a pre-stretched substrate.^{12,16,17} These were observed to have similar photovoltaic characteristics in the unstretched and stretched conditions.^{12,16} Polymer-based photovoltaic devices on plastic foil substrates with thicknesses less than 2 μm have also been shown to have equal power conversion efficiencies to those on rigid glass substrates. These can also withstand mechanical

deformation. The mechanics of failure and the stretchability and ductility of metal films on elastomer substrates have also been studied by Li^{18,19} and Xiang,²⁰ while Li and Suo²¹ have investigated the adhesion between elastomer substrates and metal films.

In an effort to understand cohesion and reliability of organic solar cells, Brand *et al.*²² have characterized the adhesive and cohesive properties of the materials and interfaces present in the layered structures of organic bulk heterojunction photovoltaic devices. They showed that adhesion and cohesion in these structures are affected by phase-separation, surface morphology, and electrochemical reactions. Dupont *et al.*^{23,24} have also improved the interfacial adhesion in bulk heterojunction solar cells by increasing the post deposition annealing temperature and time. Prior work by Bruner *et al.*²⁵ has recently shown that the cohesive properties of layers in buck heterojunction solar cells increase with increasing thickness. However, a steady decrease in power conversion efficiency was also observed with increasing thickness.

Earlier work by Tong *et al.*²⁶ has also studied the adhesion between layers that are relevant to organic solar cells and light emitting devices on rigid glass substrates. However, there have been only limited studies of adhesion on hybrid organic/inorganic light emitting devices and solar cells on flexible substrates.²⁷ This paper presents the results of an experimental study of adhesion between bi-material pairs that are relevant to organic and hybrid organic/inorganic light emitting devices and solar cells on flexible substrates. Atomic force microscopy (AFM) is used to measure the adhesion between the possible bi-material pairs that are relevant to organic and hybrid organic/inorganic light emitting devices and solar cells. The origins of the adhesion are then explored before discussing the implications of the results for the design of robust organic and hybrid organic/inorganic light emitting devices and solar cells.

II. THEORY

A. AFM force measurement

The adhesion force between two materials can be measured by contact mode AFM.^{26,28} First, the AFM tip is coated with one material. The substrate is then coated with the second material in the bi-material pair. The steps for measuring the adhesion force are illustrated in Figure 1, along with a

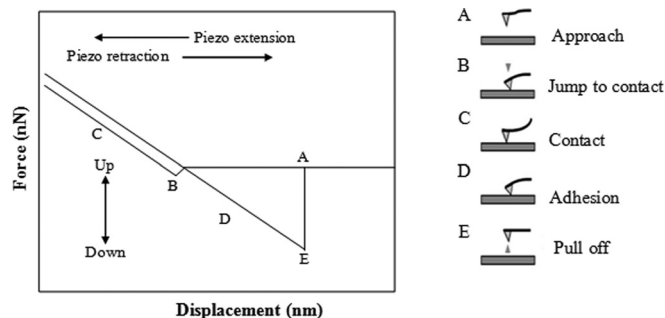


FIG. 1. Schematic force-displacement curve for various stages of AFM measurement from A to E (Ref. 26).

force-displacement curve associated with the tip deflection (A-E). The displacement of the AFM cantilever tip begins (at point A) above the substrate. As the tip is lowered towards the substrate, it will jump to contact (point B). Subsequent deflection of the tip is associated with elastic bending, as the tip is deflected (point C) to a maximum force/displacement. The tip deflection is then reversed until the tip is separated from the substrate (point E). The adhesion force, F , is determined from Hooke's law to be

$$F = -kx, \quad (1)$$

where x is the tip displacement (AE) and k is the spring constant of the AFM tip, which was measured using the thermal tune method.²⁹

B. Adhesion energy

There are several possible theories that can be used to estimate the adhesion energy. These include: the Derjaguin–Muller–Toporov (DMT) model,³⁰ the Johnson–Kendall–Robert (JKR) model,³¹ and the Maugis–Dugdale (MD) model.³² A non-dimensional parameter is determined to distinguish the use of these adhesion energy models.^{28–32} If the parameter is smaller than 0.1, the DMT model applies. If it is greater than 5, the JKR model applies. The intermediate values correspond to the MD model. The DMT model applies to cases in which there are weak interactions between stiff materials with small radii. The application of the DMT model to similar scenarios was reported initially by Rahbar *et al.*³³ This was extended by Meng *et al.*³⁴ to the study of adhesion in multilayered drug-eluting stents. The adhesion energy, γ , is related to the adhesion force, F , by the following expression:

$$\gamma_{DMT} = \frac{F_{adhesion}}{2\pi R}, \quad (2)$$

where R is the effective radius which is given by

$$R = \left(\frac{1}{R_{rms}} + \frac{1}{R_{tip}} \right)^{-1}, \quad (3)$$

where R_{rms} and R_{tip} are the radii of the average roughness of the substrate and the coated AFM tip, respectively.

III. EXPERIMENTAL PROCEDURES

A. Material processing

The layered structures of the flexible organic and hybrid organic/inorganic light emitting devices are presented in Figures 2(a) and 2(b). The flexible organic light emitting device has the PDMS/Cr/PEDOT:PSS/MEH:PPV/Al structure, while the flexible hybrid organic/inorganic light emitting device has the PDMS/Cr/PEDOT:PSS/MEH:PPV:TiO₂/Al structure. The layered structures of the flexible organic and hybrid organic/inorganic solar cells are presented in Figures 2(c) and 2(d). The flexible organic solar cell has the PDMS/Cr/PEDOT:PSS/P3HT:PCBM/Al structure. However, in the flexible hybrid solar cell, the active layer of P3HT:PCBM blend was replaced with P3HT:TiO₂ or a mixture of

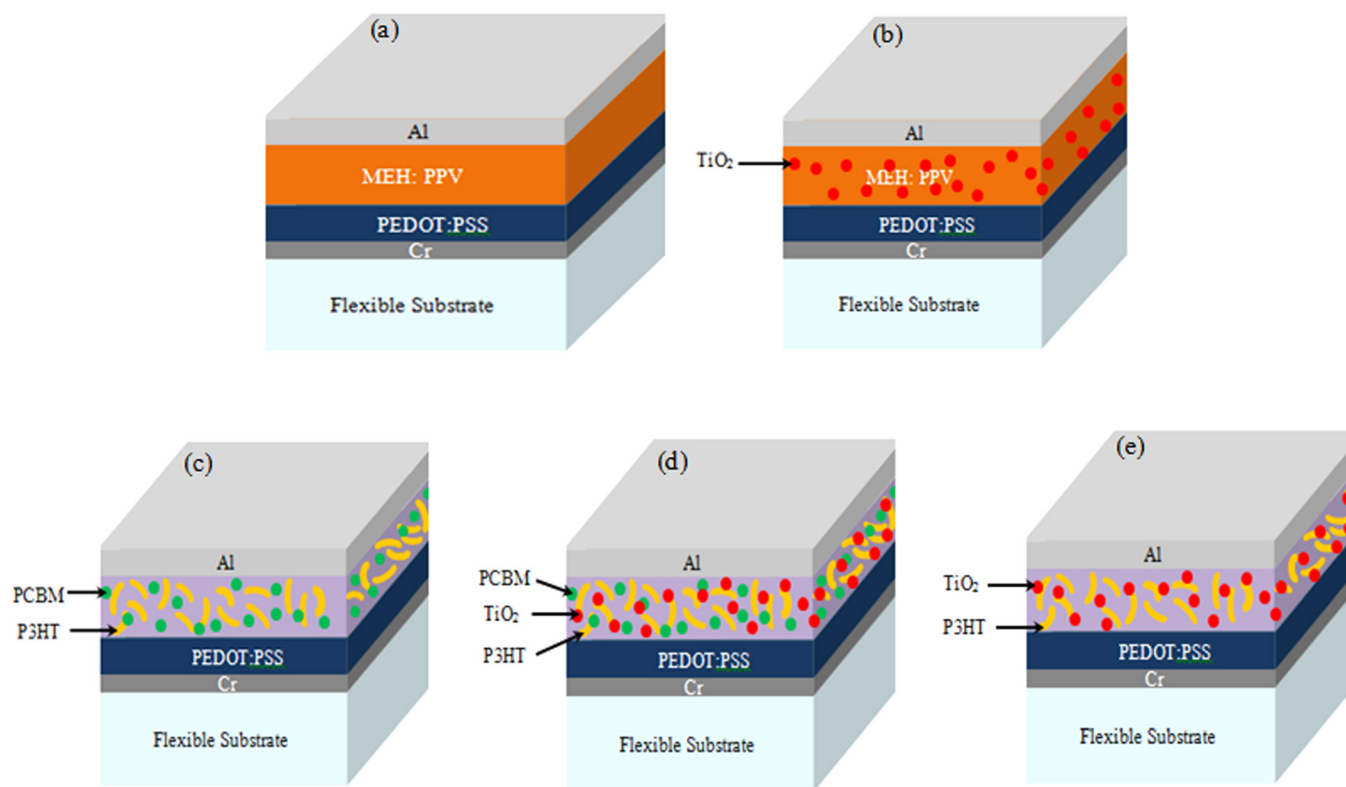


FIG. 2. Layered structures for flexible organic and hybrid light emitting device and solar cells (a) flexible organic light emitting device (b) flexible hybrid light emitting device (c) flexible organic solar cell (d and e) flexible hybrid organic/inorganic solar cell.

P3HT:PCBM:TiO₂, with the other layers being the same as those in the flexible organic solar cell.

1. Processing of the flexible organic and hybrid organic/inorganic light emitting devices

In the case of the flexible OLED, the PDMS substrate was prepared by first mixing a Slygard 184 silicone elastomer curing agent with a Slygard 184 silicone elastomer base (Dow Corning Corporation, Midland MI), with a 1:10 weight ratio. The mixture was then processed under a vacuum pressure of 6 kPa for 30 min. This was done to remove internal bubbles from the PDMS. This mixture was spin cast onto glass for 60 s. This was done at 400 revolutions per minute (rpm). The mixture was then cured for 2 h at 80 °C.

The chromium (Cr) adhesive layer of 5 nm was deposited on top of the PDMS-coated glass using an electron-beam evaporator (Denton DV 502 A, Denton Vacuum, Moorestown, NJ). Baytron P VP Al-4083 PEDOT:PSS (now Heraeus Clevis, Hanau, Germany) was filtered through a 0.2 μm filter to further improve uniformity and smoothness. The filtered mixture was spin-coated at 3000 rpm for 1 min. It was then cured at 120 °C for 5 min to remove moisture from the mixture.

The poly[2-methoxy-5-(2'-ethyl-hexyloxy)-1,4-phenylene vinylene] (MEH:PPV) (Sigma Aldrich, St. Louis, MO) was mixed with chloroform at a 5 g/l ratio. The mixture was stirred continuously for 6 h at room-temperature. It was then passed through a 0.45 μm teflon filter, prior to spin-coating at 1000 rpm for 1 min. Finally, a 100 nm thick aluminum (Al) cathode layer was thermally evaporated onto the MEH:PPV

active layer using an Edwards E306A deposition system (Edwards, Sussex, UK).

However, in the case of the flexible hybrid light emitting devices, the active layer was prepared differently, with other layers being the same as the ones in the flexible organic light emitting device. The TiO₂ nanoparticles were added into the MEH:PPV single polymer blend to form MEH:PPV:TiO₂ mixtures/composites. Subsequently, 15 mg of MEH:PPV (in 2 ml of chloroform) was mixed at room-temperature for 6 h. Consequently, 5 mg of TiO₂ was sonicated in 2 ml of chloroform for 45 min. The resulting two mixtures were then mixed and sonicated for 30 min.

2. Processing of flexible organic and hybrid organic/inorganic solar cells

In the case of the flexible organic solar cells, the PDMS substrate and Cr layer were prepared using procedures described previously in Sec. III A 1. Baytron P PEDOT:PSS obtained from H. C. Starck (now Heraeus Clevis, Hanau, Germany) was used for the electron-hole pair separation. It served as the hole extraction layer. The PEDOT:PSS solution was filtered through a 0.2 μm filter. It was then spin-coated onto the PEDOT:PSS layer for 1 min at 3000 rpm. It was cured for 5 min at 120 °C. The bulk heterojunction active layer consisted of a mixture of poly(3-hexylthiophene) (Sigma Aldrich, St. Louis, MO) and phenyl-C61-butyric acid methyl ester (Sigma Aldrich, St. Louis, MO). It was mixed with chloroform in the ratio of 1:0.8. This mixture was spin cast onto the PEDOT:PSS at 1500 rpm for 1 minute. It was then cured for 10 min at 150 °C. Finally, the aluminum (Al)

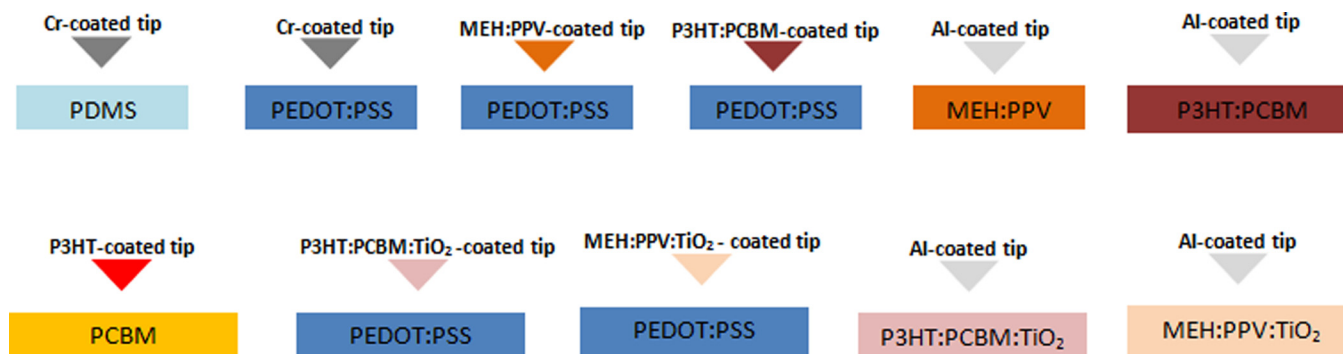


FIG. 3. Schematic of interaction between material 1 and the tip of AFM (material 2).

cathode layer was thermally evaporated onto the P3HT:PCBM active layer using an Edwards E306A deposition system (Edwards, Sussex, UK).

In the case of the flexible hybrid solar cells, the active layer was prepared differently, with other layers being prepared with the same protocols as the flexible organic solar cell. The active layer of the P3HT:TiO₂ or the P3HT:PCBM:TiO₂ blend was prepared as follows: For the P3HT:TiO₂ blend, the PCBM was replaced entirely with TiO₂ (Sigma Aldrich, St. Louis, MO). The best weight ratio of P3HT:TiO₂ blend was found to be 1:2.3.¹¹ In the case of P3HT:PCBM:TiO₂ blend, the weight ratio was chosen to be 1:0.4:0.4. This ratio replaced half the PCBM with TiO₂. The TiO₂ nanoparticles were dissolved in chlorobenzene and sonicated for at least 30 min to form a uniform solution. The TiO₂ solution was then mixed with P3HT or P3HT:PCBM solution and placed in an ultrasonic bath for an additional 30 min. The blend was then spin coated for 60 s at 150 rpm, before annealing for 10 min at 150 °C.

B. AFM adhesion experiments

Etched silicon contact mode AFM tips were purchased from Veeco Instruments (now Bruker Instruments) Woodbury, NY. The PDMS substrates were coated with Cr, while the AFM tips were coated separately with Cr and Al, using an Edwards E306A evaporation system (Edwards, Sussex, UK). The PDMS substrates were coated with Cr to improve their adhesion to PDMS substrates. PEDOT:PSS solution was then spin-coated onto Cr-coated PDMS substrates. AFM tips were dip-coated with organic (P3HT:PCBM, MEH:PPV and P3HT) and organic/inorganic (P3HT:PCBM:TiO₂, MEH:PPV:TiO₂, P3HT:TiO₂, and TiO₂) active materials. To measure the adhesion forces between the active materials and Al, both organic and hybrid organic/inorganic active materials were spin-coated onto glass substrates. PCBM was also spin-coated onto glass in the order to measure the adhesion between P3HT (coated on the AFM tip) and PCBM (coated on glass).

The AFM measurements were performed in air of a temperature range of 22–25 °C and a relative humidity range of 31%–46%. A schematic of the interaction between the substrate (material 1) and the tip of AFM (material 2) is presented in Figure 3. About ten force-displacement curves were obtained for each interaction. The force-displacement

measurements were obtained using a Digital Instruments Dimension 3000 AFM (Digital Instruments, Plainview, NY). The spring constant of each tip was measured using the thermal tune method.²⁹ The measurements were performed in a Digital Instruments Nanoscope IIIa atomic force microscope (Digital Instruments, Plainview, NY). The measurements of the tip deflections and the spring constants were then substituted into Eq. (1) to determine the adhesion forces.

Due to the high sensitivity of AFM measurements to surface roughness, the substrate roughnesses and the tip radii were measured for each of the interaction pairs. The surface roughnesses were obtained using tapping mode AFM. About 10 height and phase images of each substrate were obtained. These were used to measure the root mean squared roughnesses in areas ranging from 1 × 1 to 10 × 10 μm². The AFM tips were examined in a Scanning Electron Microscope (SEM) that was instrumented with an Energy Dispersive X-ray Spectroscopy (EDS) system (Philips FEI XL30 FEG-SEM, Hillsboro, OR). This was done before and after the AFM adhesion measurements. The tip radii were calculated from tip images obtained from SEM (Figure 4). The measurements of the surface roughness and the tip radii were then used to estimate the effective tip radii and the adhesion energies from Eqs. (3) and (2), respectively. The SEM/EDS images of the AFM tips (before and after measurements) were also used to check for any changes in the morphology

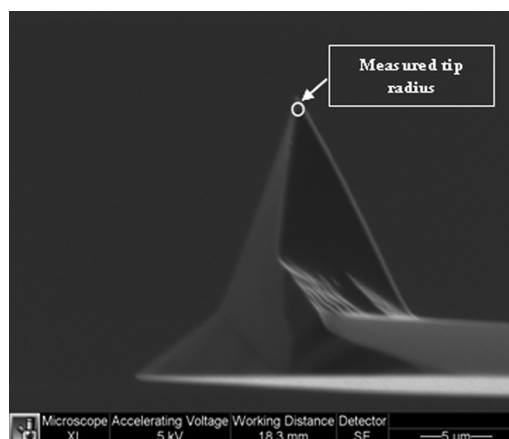


FIG. 4. SEM image of a typical AFM tip profile.

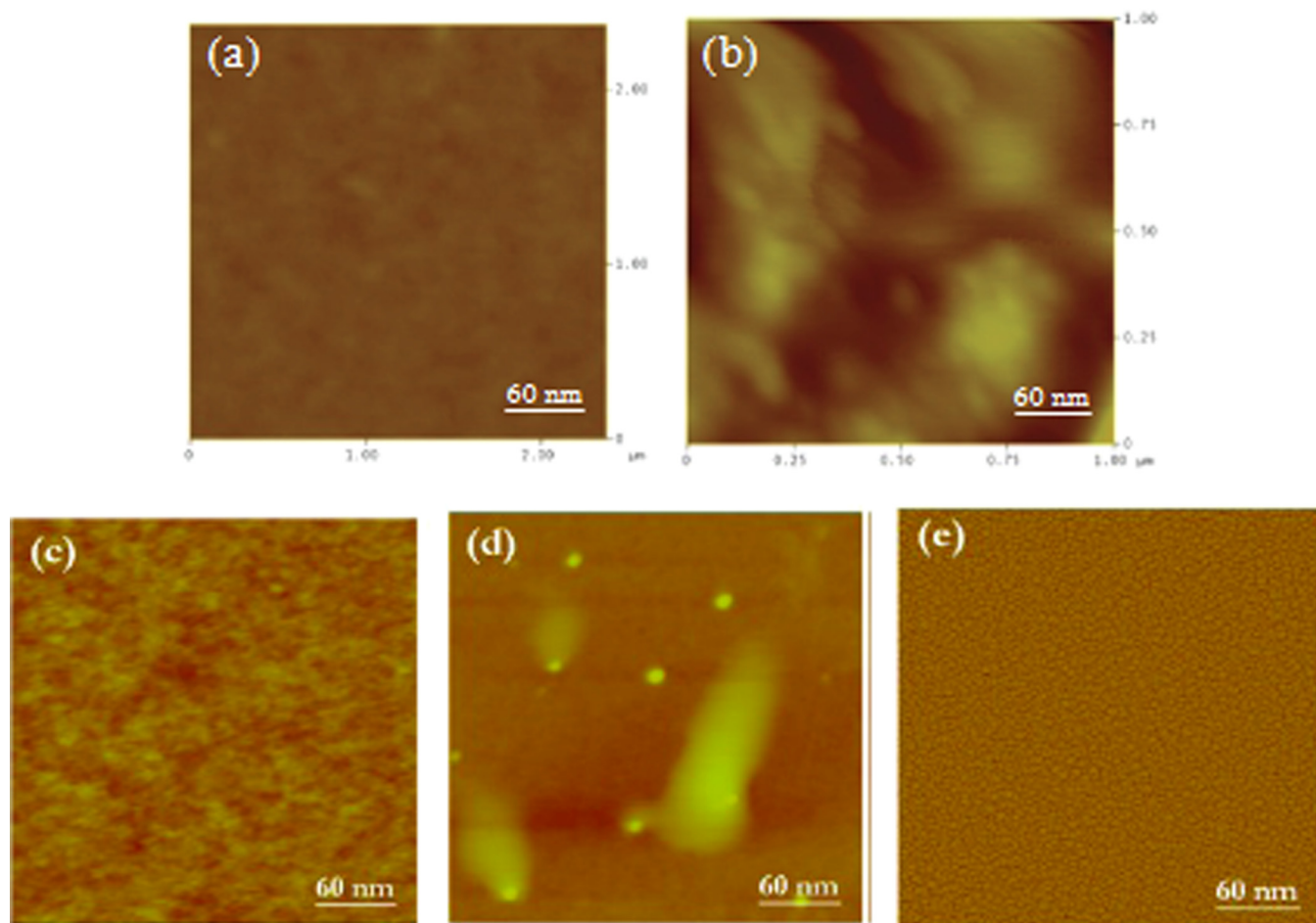


FIG. 5. AFM surface morphologies for different layers in the flexible light emitting device: (a) PDMS (b) Cr (c) Baytron P VP AL-4083 PEDOT:PSS (d) MEH:PPV (e) Al.

and atomic number contrast (composition differences) of the AFM tips after the AFM adhesion measurements. In this way, the SEM images of the AFM tips were used to check for possible occurrences of cohesive and adhesive failure.

IV. RESULTS AND DISCUSSION

A. Surface characterization

1. Surface morphologies and roughness measurements

The root mean squared (rms) surface roughnesses of the different layers in the organic light emitting device that were examined in this are presented in Figure 5. The average rms

TABLE I. Average rms roughness values for layers in the flexible light emitting device.

Surface layer	Roughness (nm)
PDMS on glass	0.6 ± 0.1
Cr	9.9 ± 2.2
PEDOT:PSS	0.6 ± 0.1
MEH:PPV	2.2 ± 0.7
Al	2.4 ± 0.4

roughness values obtained for the different layers are presented in Table I. The layers in the flexible light emitting device had low surface roughnesses that ranged from 0.6 nm to 2.4 nm, while the Cr layer had a higher roughness value of 9.9 ± 2.2 nm. It is important to note that the surface roughness values obtained for PDMS spun on glass was very low (below 1 nm). This is expected from a conformal, elastomeric polymer surface. The average tip radius of the coated tip was about 170 nm. Since the surface roughnesses were much smaller than the tip radii, it can be concluded from Eqs. (2) and (3) that the surface roughnesses dominated the adhesion energy calculations.

The different materials in the layers of the flexible solar cells exhibited different surface morphologies, as shown in Figure 6. The average rms roughness values obtained for the different layers are present in Table II. The layers in the flexible solar cell had low rms surface roughness values, ranging from 0.6 nm to 2.4 nm, while the Cr layer had higher rms roughness values of $\sim 9.9 \pm 2.2$ nm. The average tip radius of the coated tip was about 180 nm. Since the surface roughnesses were much smaller than the tip radii, it can be concluded that the surface roughnesses dominated the adhesion energy calculations. In the SEM/EDS images of the tips, no significant changes were observed. Furthermore, the highest

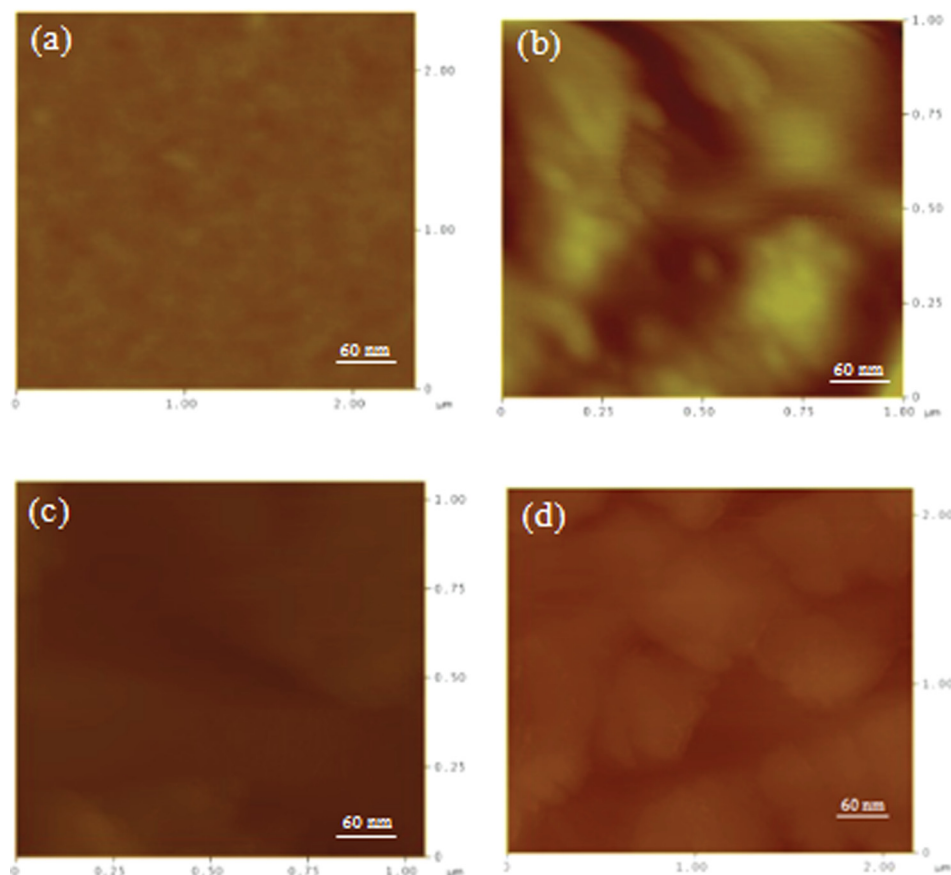


FIG. 6. AFM surface morphologies for different layers in the flexible solar cells: (a) PDMS on glass (b) Cr (c) PEDOT:PSS (d) P3HT:PCBM.

magnification SEM images did not reveal any evidence of cohesive failure. Hence, we conclude that the measured AFM pull-off forces correspond to adhesive failures.

B. Adhesion of flexible organic and hybrid organic/inorganic light emitting devices

1. Adhesion forces

The adhesion forces obtained for the bi-material pairs in the model flexible organic and hybrid light emitting device are summarized in Figure 7. These show that the adhesion force between PEDOT:PSS and MEH:PPV:TiO₂ had the highest value of 82 nN. The Cr layer also adhered well to the PDMS layer and also to the PEDOT:PSS layer. The adhesion force between PEDOT:PSS and MEH:PPV was found to be 59 nN, while the adhesion force between the MEH:PPV and the Al layer was ~ 10 nN. The addition of TiO₂ nanoparticles to the MEH:PPV increased the adhesion force between

PEDOT:PSS and MEH:PPV:TiO₂. Also, the adhesion force between the MEH:PPV:TiO₂ and Al layer was ~ 31 nN.

2. Adhesion energies

The non-dimensional parameter for the calculation of the adhesion energy was found by performing the iterative calculations to be $\sim 10^{-8}$. Since this is $\ll 0.1$,^{27,28} the DMT model applies. By taking into account of the surface roughness and the AFM tip radius, the adhesion energy can be obtained from Eqs. (2) and (3). This DMT model had been used in this way for interfacial fracture toughness calculations^{27,28,33,34} in different multilayered structures. The adhesion energy results obtained for the bi-material pairs in flexible organic and hybrid light emitting devices are summarized in Figure 8. The results show that the Cr layer adhered strongly to the PDMS substrate, with a high adhesion energy of 18.9 J/m². The adhesion energy between PEDOT:PSS and MEH:PPV was 15 J/m². After adding TiO₂ nanoparticles to the MEH:PPV single polymer blend, the adhesion energy between PEDOT:PSS and MEH:PPV:TiO₂ had a higher value of 20.8 J/m².

It is important to note here that the increase in the adhesion energy of PEDOT:PSS-MEH:PPV:TiO₂ interface can be attributed to changes in surface morphology and phase separation of MEH:PPV:TiO₂, as well as electrochemical reactions between PEDOT:PSS and MEH:PPV:TiO₂. The latter occur due to the introduction of TiO₂. Similar phenomena have been reported by Dauskardt and co-workers^{22,25} in research on P3HT:PCBM mixtures. Also, the adhesion energy between

TABLE II. Average rms roughness values for layers in the flexible solar cells.

Surface layer	Roughness (nm)
PDMS on glass	0.6 ± 0.1
Cr	9.9 ± 2.2
PEDOT:PSS	0.8 ± 0.1
P3HT:PCBM	0.7 ± 0.1
Al	2.4 ± 0.4

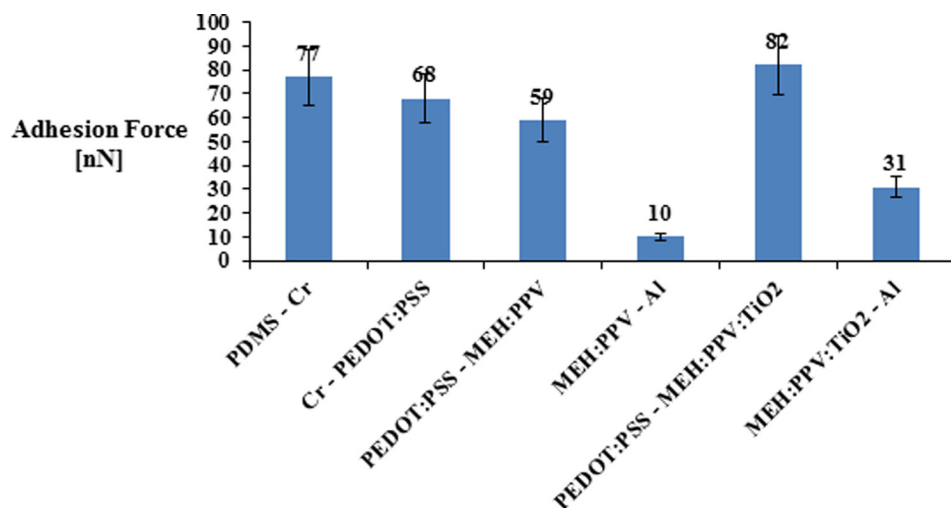


FIG. 7. Interfacial adhesion forces in flexible organic and hybrid organic/inorganic light emitting devices.

MEH:PPV and Al was 0.8 J/m^2 . Furthermore, the addition of TiO_2 nanoparticles to the MEH:PPV single polymer blend resulting in an adhesion energy between MEH:PPV:TiO₂ and Al of 5.9 J/m^2 . The hybrid light emitting device with the MEH:PPV:TiO₂ active layer, therefore, had higher adhesion energies at the two interfaces with its adjacent layers.

C. Adhesion of flexible organic and hybrid organic/inorganic solar cells

1. Adhesion forces

The adhesion forces obtained for the bi-material pairs in the model flexible organic and hybrid solar cell are summarized in Figure 9. The adhesive interactions in PEDOT:PSS-P3HT:TiO₂ and PEDOT:PSS-P3HT:PCBM:TiO₂ structures are compared with those of the PEDOT:PSS-P3HT:PCBM bi-material couples. The results show that the adhesive interactions between PEDOT:PSS and P3HT:PCBM result in the highest adhesion force of $\sim 187 \text{ nN}$. The adhesive interactions between PEDOT:PSS and P3HT:TiO₂ had the second highest adhesion force values of 69 nN , while the adhesive interactions between PEDOT:PSS and P3HT:PCBM:TiO₂ resulted in the lowest adhesion forces of $\sim 40 \text{ nN}$. The adhesion force between P3HT and TiO₂ was low, with a value of

$\sim 8 \text{ nN}$. The adhesive interactions between P3HT and PCBM resulted in an adhesion force of $\sim 23 \text{ nN}$. The adhesive interactions of P3HT:TiO₂-Al and P3HT:PCBM:TiO₂-Al were compared with that of P3HT:PCBM-Al. The adhesion force between Al and P3HT:TiO₂ was the highest (306 nN), while that between Al and P3HT:PCBM:TiO₂ had the second highest value of 140 nN . The lowest adhesion force of $\sim 50 \text{ nN}$ occurred between Al and P3HT:PCBM.

2. Adhesion energies

The non-dimensional parameter for the calculation of the adhesion energy was found by performing the iterative calculations to be $\sim 10^{-6}$, which is $\ll 0.1$.^{27,28} Since the parameter is much smaller than 0.1, the DMT model applies. By taking into account of the surface roughness and the AFM tip radius, the adhesion energies were obtained from Eqs. (2) and (3). The adhesion energy results were presented in Figure 10 for the possible bi-material pairs in the flexible organic and hybrid solar cell.

The results presented in Figure 10 show that the Cr layer adhered strongly to the PDMS substrate, with the high adhesion energy of 18.9 J/m^2 . The P3HT:PCBM layer adhered strongly to PEDOT:PSS layer, with the highest adhesion

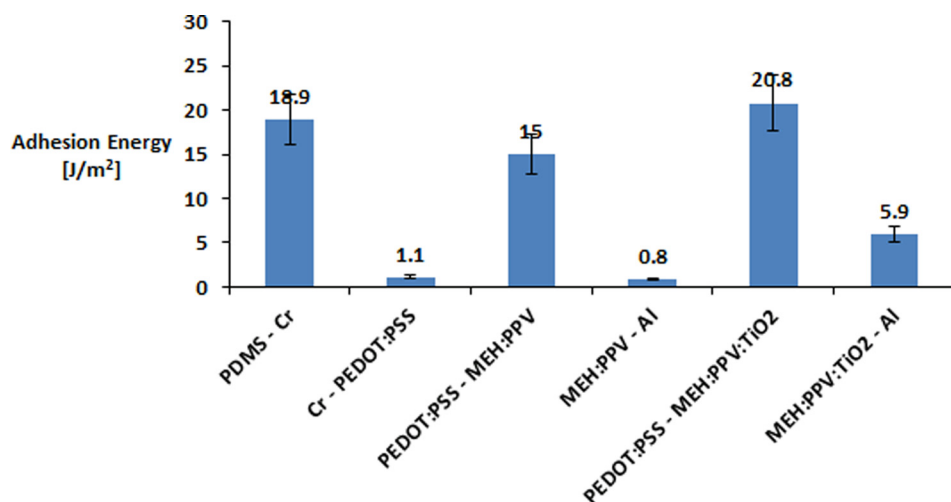


FIG. 8. Interfacial adhesion energies in flexible organic and hybrid organic/inorganic light emitting devices.

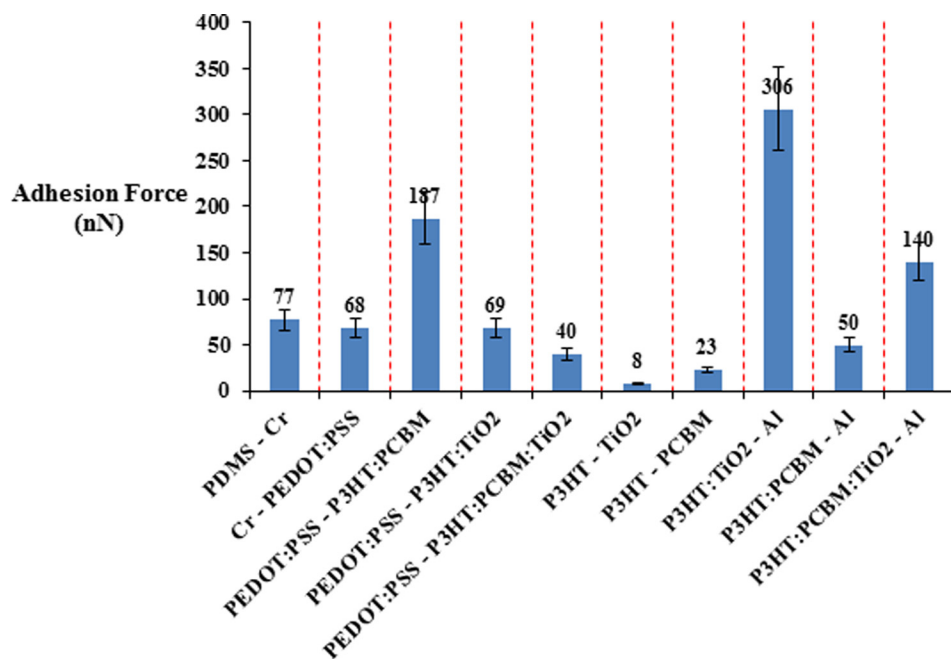


FIG. 9. Interfacial adhesion forces in flexible organic and hybrid organic/inorganic solar cell.

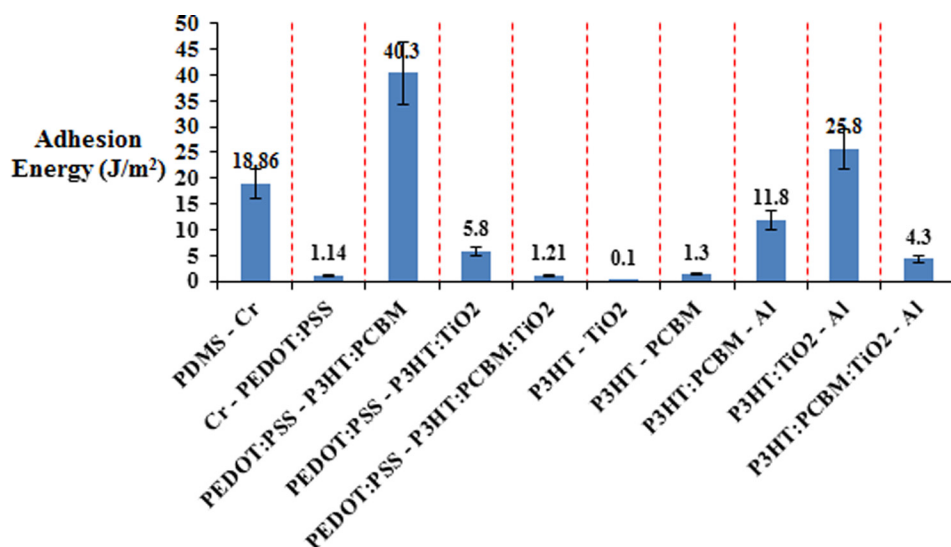


FIG. 10. Interfacial adhesion energies in flexible organic and hybrid organic/inorganic solar cell.

energy value of 40.3 J/m^2 . The high adhesion energy of the PEDOT:PSS-P3HT:PCBM interface may be due to the physical intermixing of P3HT and PSS. These react electrochemically to form P3HT^+ and PSS^- , as reported by Brand *et al.*²² and Huang *et al.*³⁵ Also, the adhesion between PEDOT:PSS and P3HT:PCBM layer was much bigger than the adhesion energies of PEDOT:PSS-P3HT:TiO₂ and PEDOT:PSS-P3HT:PCBM:TiO₂. Furthermore, the adhesion energy between PEDOT:PSS and P3HT:TiO₂ was much greater than that between PEDOT:PSS and P3HT:PCBM:TiO₂.

It is also important to note here that the reduction in adhesion energy in PEDOT:PSS-P3HT:PCBM:TiO₂ can be attributed to possible effects of electrochemical reactions, due to introduction of TiO₂ nanoparticles. This can be as a result of secondary bonds that are formed when hydrogen atoms in P3HT:PCBM are attracted to oxygen atoms in TiO₂ during the chemical reactions.

The adhesion energy between P3HT and TiO₂ had the lowest with a value of 0.1 J/m^2 . The adhesion energy between P3HT and PCBM was also small (1.3 J/m^2). This is in the range of the values reported by Brand *et al.*²² Furthermore, considering the adhesion energies between Al and different active layers, the adhesion energy between Al and P3HT:TiO₂ was the highest (with a value of 25.8 J/m^2). This was greater than the adhesion energies of the Al-P3HT:PCBM:TiO₂ and the Al-P3HT:PCBM structure. Hence, from the robustness point of view, the active layer of P3HT:TiO₂ blend was more robust than the active layer consisting of P3HT:PCBM:TiO₂ blends.

V. SUMMARY AND CONCLUDING REMARKS

In this paper, a force microscopy technique was used to measure the adhesion between possible bi-material pairs that

are relevant to flexible organic and hybrid organic/inorganic light emitting devices and solar cells. A summary of the salient conclusions arising from this work is presented below.

1. The AFM technique provides a simple method for the ranking of the adhesion forces and energies between different layers in flexible organic and hybrid organic/inorganic light emitting devices and solar cells. This could facilitate the future design of robust flexible organic and hybrid organic/inorganic light emitting devices and solar cells.
2. In the case of the hybrid organic/inorganic light emitting device in which the active layer of MEH:PPV blend is replaced by MEH:PPV:TiO₂ mixture, the MEH:PPV:TiO₂ active layer had higher adhesion energies with the adjacent layers (PEDOT:PSS and Al). Therefore, from the robustness point of view, the blended active layer of MEH:PPV:TiO₂ adheres better to the adjacent Al and PEDOT:PSS layers than the active layer consisting of MEH:PPV.
3. In the case of the hybrid organic/inorganic solar cell in which the active layer of P3HT:PCBM blend is replaced with P3HT:TiO₂ or P3HT:PCBM:TiO₂ mixture, the P3HT:PCBM layer adhered better to the adjacent PEDOT:PSS and Al layers. However, although the incorporation of TiO₂ particles into the active layers has the potential of improving charge transport, the TiO₂ in the P3HT:TiO₂ layer reduces the adhesion to the adjacent PEDOT:PSS layer. Furthermore, the P3HT:PCBM:TiO₂ layer adheres poorly to the two adjacent layers (PEDOT:PSS and Al).
4. The incorporation of TiO₂ nanoparticles into the active layers of bulk heterojunction (P3HT:PCBM) organic solar cells reduces the adhesion to the adjacent hole transport and cathode layers. This is attributed to the potential effects of electrochemical reactions that are associated with the introduction of TiO₂. Hence, the improvements in charge transport facilitated by TiO₂ must, therefore, be balanced against potential reductions in the adhesion that might occur as a result of the incorporation of TiO₂ nanoparticles into the active layers of bulk heterojunction solar cells.

ACKNOWLEDGMENTS

The research was supported by the National Science Foundation (DMR 0231418), Princeton University, the Princeton Grand Challenge Program, The World Bank STEP B Program, African Centers of Excellence of the World Bank, the African Capacity Building Foundation, and the African Development Bank. The authors are grateful to these organizations for their financial support.

- ¹S. R. Forrest, *Org. Electron.* **4**, 45 (2003).
- ²Heliatek, Dienstag, 06 December (2011).
- ³C. Kim, P. E. Burrows, and S. R. Forrest, *Science* **288**, 831 (2000).
- ⁴J. W. P. Hsu, *Mater. Today* **8**, 42 (2005).
- ⁵S. F. Lim, L. Ke, W. Wang, and S. J. Chua, *Appl. Phys. Lett.* **78**, 2116 (2001).
- ⁶D. Y. Momodu, T. Tong, M. G. Zebaze Kana, A. V. Chioh, and W. O. Soboyejo, *J. Appl. Phys.* **115**, 084504 (2014).
- ⁷M. D. McGehee, *Mater. Res. Soc. Bull.* **34**, 95 (2009).
- ⁸C. Y. Kuo, W. C. Tang, T. F. Guo, and D. Z. Jeng, *Appl. Phys. Lett.* **93**, 033307 (2008).
- ⁹H.-J. Her, J.-M. Kim, C. J. Kang, and Y.-S. Kim, *J. Phys. Chem. Solids* **69**, 1301 (2008).
- ¹⁰S. Yodyingyong, X. Zhou, Q. Zhang, D. Triampo, J. Xi, K. Park, B. Limketkai, and G. Cao, *J. Phys. Chem. C* **114**(49), 21851 (2010).
- ¹¹C. Y. Kwong, A. B. Djuric, P. C. Chui, K. W. Cheng, and W. K. Chan, *Chem. Phys. Lett.* **384**, 372 (2004).
- ¹²D. J. Lipomi, B. C.-K. Tee, M. Vosgueritchian, and Z. Bao, *Adv. Mater.* **23**, 1771 (2011).
- ¹³G. Dennler, C. Lungenschimied, A. Labouret, H. Neugebauer, and N. S. Sariciftci, *J. Mater. Res.* **20**(12), 3224 (2005).
- ¹⁴J. Lee, J. Wu, M. Shi, J. Yoon, S.-I. Park, M. Li, Z. Liu, Y. Huang, and J. A. Rogers, *Adv. Mater.* **23**, 986 (2011).
- ¹⁵Z. Yu, X. Niu, Z. Liu, and Q. Pei, *Adv. Mater.* **23**, 3989 (2011).
- ¹⁶T. Sekitani, H. Nakajima, H. Maeda, T. Fukushima, T. Aida, K. Hata, and T. Someya, *Nature Mater.* **8**, 494 (2009).
- ¹⁷D. J. Lipomi, J. A. Lee, M. Vosgueritchian, B. C.-K. Tee, J. A. Bolander, and Z. Bao, *Chem. Mater.* **24**, 373 (2012).
- ¹⁸T. Li, Z. Y. Huang, Z. C. Xi, S. P. Lacour, S. Wagner, and Z. Suo, *Mech. Mater.* **37**, 261 (2005).
- ¹⁹T. Li, Z. Huang, Z. Suo, S. P. Lacour, and S. Wagner, *Appl. Phys. Lett.* **85**(16), 3435 (2004).
- ²⁰Y. Xiang, X. Chen, and J. J. Vlassak, *Mater. Res. Soc. Symp. Proc.* **695**, L4.9 (2002).
- ²¹T. Li and Z. Suo, *Int. J. Solids Struct.* **44**, 1696 (2007).
- ²²V. Brand, C. Bruner, and R. H. Dauskardt, *Sol. Energy Mater. Sol. Cells* **99**, 182 (2012).
- ²³S. R. Dupont, M. Oliver, F. C. Krebs, and R. H. Dauskardt, *Sol. Energy Mater. Sol. Cells* **97**, 171 (2012).
- ²⁴S. R. Dupont, E. Voroshazi, P. Heremans, and R. H. Dauskardt, *Org. Electron.* **14**, 1262 (2013).
- ²⁵C. Bruner and R. Dauskardt, *Macromolecules* **47**, 1117 (2014).
- ²⁶T. Tong, B. Babatope, S. Admassie, J. Meng, O. Akwogu, W. Akande, and W. O. Soboyejo, *J. Appl. Phys.* **106**, 083708 (2009).
- ²⁷T. Michelle Tong, "Adhesion and interfacial fracture: From organic light emitting devices and photovoltaic cells to solar lanterns for developing regions," Ph.D. Thesis (Princeton University, 2012).
- ²⁸O. Akogwu, D. Kwabi, A. Munhutu, T. Tong, and W. O. Soboyejo, *J. Appl. Phys.* **108**, 123509 (2010).
- ²⁹Veeco Instruments Inc., Improving the Accuracy of AFM Measurements, the Thermal Tune Solution, Bruker Corporation, Billerica, MA, 2005.
- ³⁰B. V. Derjaguin, V. M. Muller, and Y. P. Toporov, *Prog. Surf. Sci.* **45**, 131 (1994).
- ³¹K. L. Johnson, K. Kendall, and A. D. Roberts, *Math. Phys. Sci. Ser. A* **324**, 301 (1971).
- ³²D. Maugis, *J. Colloid Interface Sci.* **150**, 243 (1992).
- ³³N. Rahbar, K. Wolf, A. Orana, R. Fennimore, Z. Zong, J. Meng, G. Papandreou, C. Maryanoff, and W. Soboyejo, *J. Appl. Phys.* **104**, 103533 (2008).
- ³⁴J. Meng, A. Orana, T. Tan, K. Wolf, N. Rahbar, H. Li, G. Papandreou, C. Maryanoff, and W. Soboyejo, *J. Mater. Res.* **25**(4), 641 (2010).
- ³⁵D. M. Huang, S. A. Mauger, S. Frieddrich, S. J. George, D. Dumitriu-LaGrange, S. Yoon, and A. J. Moule, *Adv. Funct. Mater.* **21**, 1657 (2011).